



Coal permeability maps under the influence of multiple coupled processes

Shouwen Zhang^{a,b}, Jishan Liu^{c,d,*}, Mingyao Wei^a, Derek Elsworth^e

^a State Key Laboratory of Geomechanics and Geotechnical Engineering, Institute of Rock and Soil Mechanics, Chinese Academy of Sciences, Hubei 430071, China

^b University of Chinese Academy of Sciences, Beijing 100049, China

^c School of Mechanical and Chemical Engineering, The University of Western Australia, 35 Stirling Highway, WA 6009, Australia

^d Beijing Key Laboratory for Precise Mining of Intergrown Energy and Resources, China University of Mining and Technology, Beijing 100083, China

^e Department of Energy and Mineral Engineering, G3 Centre and Energy Institute, The Pennsylvania State University, University Park, PA 16802, USA

ARTICLE INFO

Keywords:
Permeability map
Overlapping approach
Global strain
Local effects
Coupled processes

ABSTRACT

The evolution of coal permeability has been studied exhaustively and a broad array of permeability models developed. These models are normally derived under the assumption of fluid pressure equilibrium between matrix and fractures. Under this assumption, these models define coal permeability as a function of either gas pressure or effective stress. However, experimental observations indicate that coal permeability may change significantly under a constant observed gas pressure or assumed effective stress. The goal of this study is to resolve this contradiction. In this study, we hypothesize that coal permeability is closely related to the expansion of gas-invaded area/volume as a concentration front propagates from the fracture wall into the matrix. When this invaded volume/area is localized around the fracture, the gas-induced swelling reduces the coal permeability. When the area spreads throughout the entire matrix, gas-induced swelling may increase coal permeability. This important mechanism of transition from local (to the fracture) swelling to global (into the matrix medium) swelling is incorporated into an overlapping dual permeability approach. In this approach, the coal is characterized by a well-defined macroscopic model consisting of four overlapping/interpenetrating continua comprising: (1) coal matrix system; (2) coal fracture system; (3) gas flow in the matrix system; and (4) gas flow in the fracture system. These four continua are connected through a full set of cross-coupling relations, including (1) local force balance between the matrix and the fracture; (2) local deformation compatibility between the matrix and the fracture; and (3) mass exchange between the matrix and the fracture. We apply this approach to generate coal permeability maps under the influence of multiple coupled processes. For a particular coal sample, the permeability is bounded by the solutions for the free-swelling case (upper bound) and for the constant volume case (lower bound). The variations of permeability between the upper and lower bounds under a constant gas pressure are determined by the dynamics of matrix-fracture interactions. Current experimental measurements are bounded by these limits depending on the state of equilibrium between matrix and fractures. These model results are verified against experimental observations reported in the literature.

1. Introduction

Permeability is one of the most important properties of coal that determines the extraction of coalbed methane (CBM). CBM production begins with dewatering the coal seam to reduce the reservoir pressure and liquid saturation. Then the adsorbed gas in the coal matrix desorbs from the pore surfaces, and diffuses into the fractures and flows into the coal cleats towards the production wells as free phase gas. When the gas desorbs/adsorbs from the matrix, the matrix may shrink/swell. Matrix shrinkage/swelling changes the fracture apertures. Thus, CBM extraction triggers a series of interactions between coal matrix and fractures. These interactions modify the coal permeability during CBM extraction.

These modifications are sufficiently large that representative permeability models have to be used for the evaluation of CBM extraction.

Over the past few decades, a variety of permeability models have been developed to define the impact of shrinkage/swelling. Earlier models (Gray and Reservoir engineering in coal seams, 1987; Palmer and Mansoori, 1996; Somerton et al., 1975; Zhang et al., 2008) were developed based on the theory of single poroelasticity. By their very nature, these models could not include the interaction between the coal matrix and the fracture. In order to overcome this limitation, dual porosity and dual permeability models were developed based on the theory of dual poroelasticity (Bai et al., 1993; Wu et al., 2010, 2011; Lu and Connell, 2011; Peng et al., 2014; Wang et al., 2013; Pan and

* Corresponding author at: School of Mechanical and Chemical Engineering, The University of Western Australia, 35 Stirling Highway, WA 6009, Australia.
E-mail address: jishan.liu@uwa.edu.au (J. Liu).

Connell, 2007; Lu and Connell, 2007). In these models, the interactions between coal matrix and fractures are normally defined by the gas mass exchange term alone, and the mechanical interactions are not included. A common field of total strain was used for the ensemble matrix and fracture system. Under this condition, the fracture and matrix strains could only be approximated by an averaged pore fluid pressure in the matrix, this in turn defining fracture closure. It is this fracture strain component that determines the coal permeability. A number of approaches have been developed to overcome this limitation. The concept of pore strain was developed to define the impact of coal shrinkage/swelling (Lu and Connell, 2010). It was demonstrated that the pore strain is much larger than the coal matrix swelling strain. Furthermore, a strain-splitting approach was developed (Liu et al., 2010a; Guo et al., 2014; Peng et al., 2016; Liu et al., 2017). In this approach, the internal swelling strain is divided into two parts: one for the matrix and the other for the fracture. Only the component for the fracture contributes to the modification of coal permeability. This approach demonstrates the importance of the fracture strain but fails to fully resolve the problem because it does not consider the true matrix-fracture interactions. This failure is apparent (Liu et al., 2011a) for the primary reason that coal permeability is also related to the non-equilibrium expansion of the coal swelling volume as the pressure pulse propagates from the fracture wall into the matrix (Qu et al., 2014). In order to include this mechanism, the concept of a transition in coal deformation from local swelling to global swelling was developed (Liu et al., 2011b). This concept was verified by experimental observations (Liu et al., 2016). As a logical extension of these previous studies, this important mechanism is incorporated into the overlapping approach detailed here.

In this approach, the coal is characterized by a well-defined macroscopic model consisting of four interpenetrating continua: (1) coal matrix system; (2) coal fracture system; (3) gas flow in the matrix system; and (4) gas flow in the fracture system. The governing equations and boundary conditions are derived by applying the laws of continuum solid/flow mechanics to each continuum. These four continua are connected through a full set of cross-coupling relations, including (1) local force balance between the matrix and the fracture; (2) local deformation compatibility between the matrix and the fracture; and (3) mass exchange between the matrix and the fracture.

2. Conceptual model

Coal is a typical dual porosity/permeability medium containing porous matrix and fractures. The gas flows rapidly in the fractures and diffuses slowly in the matrix. Gas flow and diffusion have a significant influence on the strains in the coal matrix and fractures which are directly related to the evolution of porosity and permeability. In this section, we apply an overlapping continua approach to characterize the interactions between the two systems - the matrix and fracture systems - and to explain why permeability changes as a function of the interactions between the two-solid media.

As shown in Fig. 1(a), we represent coal as four overlapping and interacting physical fields: (1) matrix deformation; (2) fracture deformation; (3) gas flow in the matrix; and (4) gas flow in the fracture. The governing equations and boundary conditions are derived by applying the laws of continuum solid/flow mechanics to each continuum. These four continua are connected through a full set of cross-coupling relations, including (1) local force balance between the matrix and the fracture; (2) local deformation compatibility between the matrix and the fracture; and (3) gas mass exchange between the matrix and the fracture.

Based on the conceptual model above, Fig. 1(b)–(e) illustrate how coal permeability and porosity are related to the effective diameter of the illustrative grains, d_m , d_f . In these figures, we represent the fracture as blue block consisted of blue spheres and the matrix as black block consisted of black spheres. The diameter of blue spheres is larger than the black spheres. This indicates that the fractures have a larger

porosity than the matrix (Chilingar, 1964; Wang et al., 2017). σ represents a constant confining pressure. Δ_f represents the swelling of the fracture and Δ_m represents the swelling of the matrix.

Key physical processes include gas flow process in the fracture and the gas diffusion process from fracture to matrix. Initially, there is no gas in either fracture or matrix and the differential pressure between them is zero. Due to the high permeability of the fracture, gas flows into the fracture quickly while the pressure in the matrix remains to zero. As time progresses, the differential pressure gradually increases, which triggers gas diffusion from the fracture into the matrix. When fracture and matrix eventually achieve a final pressure equilibrium, the differential pressure is again zero. From the initial equilibrium to the final equilibrium, the differential pressure tracks from zero to a maximum then to zero. Because of the very large contrast between matrix permeability and fracture permeability, this process may last over a very long period. This is why this transient process must be considered.

3. Governing equations

We define a full set of field equations that govern the deformations of the matrix and fractures and gas flow and transfer in and between them. Originally, we develop the governing equations for the matrix based on previous work (Zhang et al., 2008). These derivations are based on the following assumptions: (a) matrix and fractures are homogeneous, isotropic and elastic; (b) strains are much smaller than the matrix block length scale; (c) gas contained within the pores is ideal, and its viscosity is constant under isothermal conditions; (d) the rate of gas flow through the coal is defined by Darcy's law. These four continua are connected through a full set of cross-coupling relations, including (1) local force balance between matrix and fractures; (2) local deformation compatibility between matrix and fractures; and (3) mass exchange between matrix and fractures. It is these local cross-couplings that determine the unique characteristics of this approach.

The mechanical properties of the matrix and fractures are very different. The response of the coal is controlled by the full coupling of different physical fields: (a) solid deformation of coal fractures, (b) solid deformation of the coal matrix, (c) gas flow in the fracture, (d) gas diffusion in the matrix. These formulae are correlative dependent with their interplay controlled by material properties. To better reveal the interactions between matrix and fractures, the two solid deformation equations are derived independently, based on single poroelasticity, rather than use the smeared equations that combine deformations.

3.1. Governing equations of matrix and fracture deformation

The equilibrium equation for matrix and fracture is defined as

$$\sigma_{ij,i} + f_j = 0 \quad (1)$$

The strain-displacement relation is expressed as

$$\varepsilon_{ij} = \frac{1}{2}(u_{i,j} + u_{j,i}) \quad (2)$$

Based on poroelastic theory (Detournay and Cheng, 1993), by making an analogy between thermal contraction and matrix shrinkage and by considering the pressure differential (Zhang et al., 2008; Ramandi et al., 2016), the constitutive relation for matrix and fracture deformation can be defined as

$$\varepsilon_{mij} = \frac{1}{2G_m}\sigma_{ij} - \left(\frac{1}{6G_m} - \frac{1}{9K_m}\right)\sigma_{kk}\delta_{ij} + \frac{\alpha}{3K_m}P_m\delta_{ij} - \frac{1}{3K_m}\Delta P\delta_{ij} + \frac{\varepsilon_{ms}}{3}\delta_{ij} \quad (3-1)$$

$$\varepsilon_{fij} = \frac{1}{2G_f}\sigma_{ij} - \left(\frac{1}{6G_f} - \frac{1}{9K_f}\right)\sigma_{kk}\delta_{ij} + \frac{\beta}{3K_f}P_f\delta_{ij} + \frac{1}{3K_f}\Delta P\delta_{ij} + \frac{\varepsilon_{fs}}{3}\delta_{ij} \quad (3-2)$$

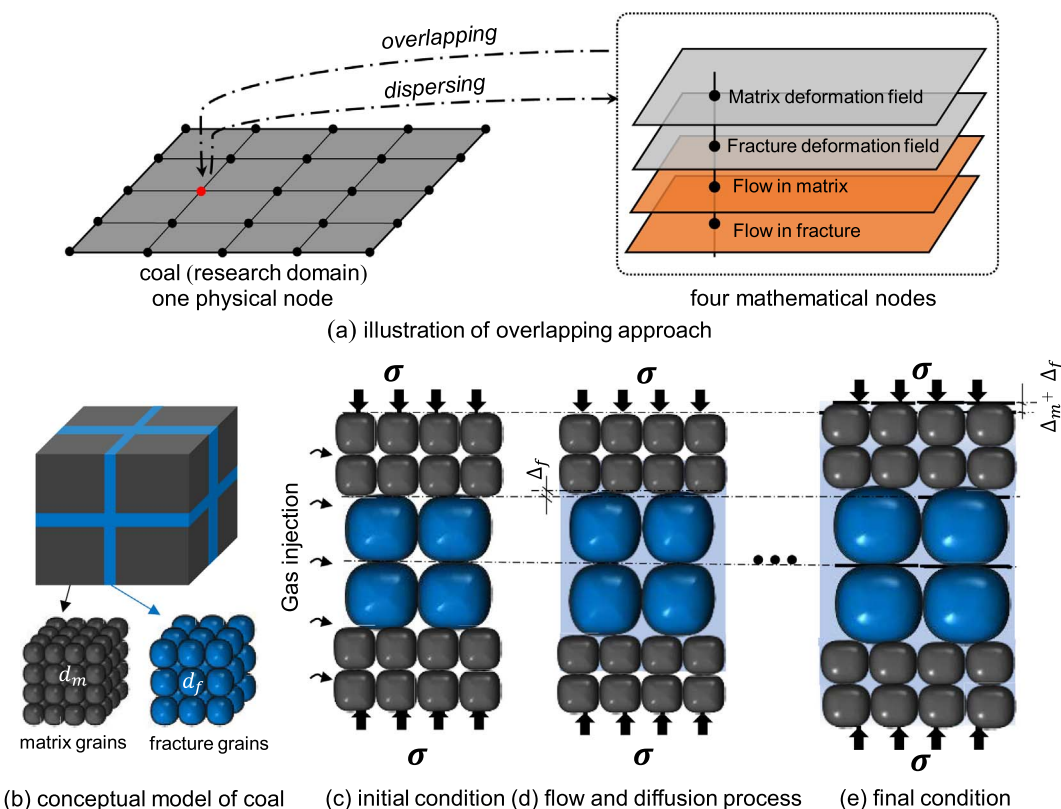


Fig. 1. Schematic diagram of the conceptual model accommodating gas injection: (a) the concept of overlapping continua; (b) idealization of coal as a dual porosity medium where gray block represents the matrix system and blue block represents the fracture system; (c) the initial equilibrium condition; (d) the flow and (e) the diffusion process. (For interpretation of the references to colour in this figure legend, the reader is referred to the web version of this article.)

where $G_m = E_m/2(1 + \nu_m)$ and $G_f = E_f/2(1 + \nu_f)$ are the shear modulus of matrix and fracture, $K_m = E_m/3(1 - 2\nu_m)$ and $K_f = E_f/3(1 - 2\nu_f)$ are the bulk modulus of matrix and fracture, E_m , E_f and ν_m , ν_f are Young's modulus and Poisson ratio of matrix and fracture, respectively. α and β are the Biot coefficient, P_m and P_f are pore pressure in matrix and fracture, σ_{kk} is total stress, ε_{ms} and ε_{fs} are the gas sorption-induced strain in matrix and fracture, ΔP is the differential pressure between fracture and matrix ($\Delta P = P_f - P_m$), δ_{ij} is the Kronecker delta.

Applying the Langmuir isotherm, the sorption-induced volumetric strain of matrix and fracture can be defined as (Harpalani and Schraufnagel, 1990)

$$\varepsilon_{ms} = \varepsilon_L \frac{P_m}{P_L + P_m} \quad (4)$$

$$\varepsilon_{fs} = \varepsilon_L \frac{P_f}{P_L + P_f} \quad (5)$$

where ε_L is the Langmuir strain constant and P_L is the Langmuir pressure constant.

Coal can be seen as a combination between a matrix medium and fracture network. Gas flow regimes in the matrix and fracture progress on different temporal scales, as illustrated in Fig. 2.

For an REV, the stress states at point 1 (yellow point) and point 2 (red point) are different. The local total stresses applied on matrix and fracture are related to time:

$$\sigma_{lmt} = \sigma + \Delta P(t) \quad (6.1)$$

$$\sigma_{lft} = \sigma - \Delta P(t) \quad (6.2)$$

Where σ_{lmt} is the total stress applied on the matrix, σ_{lft} is the total stress applied on the fracture, σ is the confining stress on the outside boundary, $\Delta P(t) = P_f(t) - P_m(t)$ is the differential pressure in the local area. Therefore, the general effective stress principle can be developed

as:

$$\sigma_{lmt} = \sigma + \Delta P(t) = \sigma_{me} + \alpha P_m \quad (6.3)$$

$$\sigma_{lft} = \sigma - \Delta P(t) = \sigma_{fe} + \beta P_f \quad (6.4)$$

The local effective stresses are not only affected by pore pressures in the matrix and fracture but also influenced by the changes of local total stress. This item considers the counter interaction between matrix and fracture when gas begins to diffuse into the matrix. Because of different flow regimes in the matrix (diffusion) and fracture (Darcy flow), the time scales are strongly different. Stress states at local areas within the coal are different with those in the entire coal. The local total stress varies with pore pressure gradient. Therefore, the deformation of the matrix grains is controlled by Eq. (6.5).

$$\sigma + \Delta P(t) = \sigma_{me} + \alpha P_m \quad (6.5)$$

where the left item is defined in this paper as local total stress which is stress gradient-related to differential pore pressure gradient. When coal is under a local stress state, the total stress is $\sigma + \Delta P(t)$, and when coal under a global stress state, there is no differential pore pressure and the total stress is σ . σ is the confining stress, σ_{me} is the effective stress component in the matrix. And from Eqs. (3), (4) and (6.5), the volumetric strain of the matrix can be expressed as

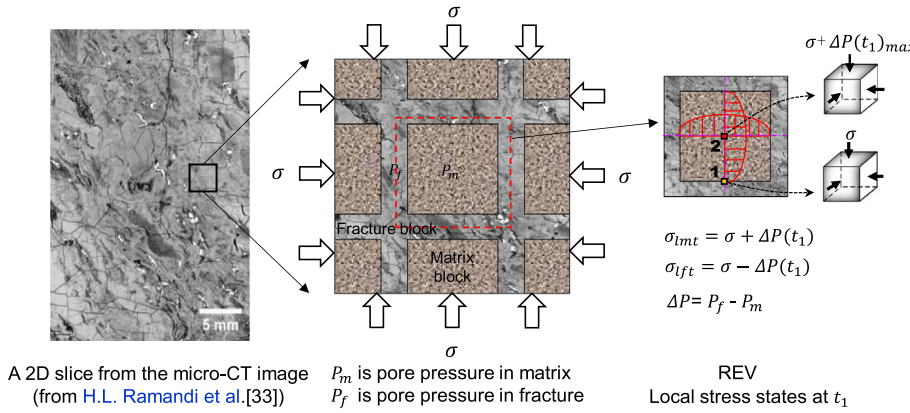
$$\varepsilon_{mv} = -\frac{1}{K_m} [\bar{\sigma} - \alpha P_m + \Delta P(t)] + \varepsilon_{ms} \quad (7)$$

where $\bar{\sigma} = -\sigma_{kk}/3$ is the mean compressive stress.

Similarly, the deformation of the fracture is controlled by

$$\sigma - \Delta P(t) = \sigma_{fe} + \beta P_f \quad (8)$$

where $-\Delta P(t)$ is the local differential pore pressure and σ_{fe} is the effective stress component of the fracture. And from Eqs. (3), (5) and (8), we can obtain the volumetric strain of the fracture as



$$\varepsilon_{fv} = -\frac{1}{K_f} [\bar{\sigma} - \beta P_f - \Delta P(t)] + \varepsilon_{fs} \quad (9)$$

Combining Eqs. (1), (2) and (3) yields the general Navier-type equation for matrix and fracture:

$$G_m u_{i,kk} + \frac{2G_m}{1-2\nu} u_{k,ki} - \alpha P_{m,i} + \Delta P_{,i} - K_m \varepsilon_{ms,i} + F_i = 0 \quad (10)$$

$$G_f u_{i,kk} + \frac{2G_f}{1-2\nu} u_{k,ki} - \beta P_{f,i} - \Delta P_{,i} - K_f \varepsilon_{fs,i} + F_i = 0 \quad (11)$$

Above all, Eqs. (10) and (11) are the governing equations for deformation of the coal matrix and fracture. These are cross coupled by the local differential force, ΔP , which reflects the interaction between matrix and fracture.

3.2. Permeability model for matrix

Gas flow in the matrix follows Darcy's law, so the equation for mass transfer of the gas in the matrix is defined as

$$\frac{\partial m_m}{\partial t} + \nabla \cdot \left(-\frac{k_m}{\mu} \rho_{gm} \nabla P_m \right) = Q_{mf} \quad (12)$$

where $m_m = \phi_m \rho_{gm} + \rho_{ga} \rho_c \frac{V_L P_m}{P_m + P_L}$ is the gas content in the matrix including free-phase gas and adsorbed gas, k_m is permeability of matrix, μ is the dynamic viscosity of the gas, ρ_g is the gas density at standard conditions, $\rho_{gm} = \frac{M_g}{RT} P_m$ is the gas density in the matrix (M_g is the molecular mass of gas, R is the universal gas constant, T is the absolute gas temperature), and Q_{mf} is gas mass transfer from fracture to matrix.

The typical relationship between porosity and permeability is the cubic law (Liu et al., 2011b)

$$\frac{k_m}{k_{m0}} = \left(\frac{\phi_m}{\phi_{m0}} \right)^3 \quad (13)$$

and the porosity of the matrix is related to the effective strain of the matrix as (Liu et al., 2011a)

$$\frac{\phi_m}{\phi_{m0}} = 1 + \frac{\alpha}{\phi_{m0}} \Delta \varepsilon_{me} \quad (14)$$

where ϕ_{m0} is the initial matrix porosity and ϕ_m is the current matrix porosity.

As mentioned in the conceptual model, the effective strain is not only interrelated to the matrix global strain but also the local force induced by the differential pressure between fracture and matrix. The effective volumetric strain increment is

$$\Delta \varepsilon_{me} = \Delta \varepsilon_{mv} + \Delta \varepsilon_{ms} - \frac{P_f - P_m}{K_m} - c_{lm} \Delta \varepsilon_{fs} \quad (15)$$

where the first item represents the global strain - obtained from the

Fig. 2. Time-dependent stress transfer within a representative elementary volume (REV). (For interpretation of the references to color in this figure, the reader is referred to the web version of this article.)

governing equation of mechanical deformation of the matrix. The second item represents the sorption-induced strain of the matrix. The third item represents the local strain induced by the change in local total stress and the last item represents the local strain induced by local sorption-induced strain of the fracture and $c_{lm} = \frac{P_f - P_m}{\Delta P_{max} K_m}$ is defined as local strain coefficient.

Substituting Eqs. (14) and (15) into Eq. (13), we obtain the permeability model for the matrix as

$$\frac{k_m}{k_{m0}} = \left[1 + \frac{\alpha}{\phi_{m0}} \left(\Delta \varepsilon_{mv} + \Delta \varepsilon_{ms} - \frac{P_f - P_m}{K_m} - c_{lm} \Delta \varepsilon_{fs} \right) \right]^3 \quad (16)$$

3.3. Gas flow in fractures

The gas flow regime within the natural fractures also obey Darcy's law. The equation for mass balance of the gas is defined as

$$\frac{\partial m_f}{\partial t} + \nabla \cdot \left(-\frac{k_f}{\mu} \rho_{gf} \nabla P_f \right) = -Q_{mf} \quad (17)$$

where $m_f = \phi_f \rho_{gf} + \rho_g \rho_c \frac{V_L P_f}{P_f + P_L}$ is the gas content in the fracture including free-phase gas and adsorbed gas, ϕ_f is fracture porosity, ρ_g is the gas density at standard conditions, $\rho_{gf} = \frac{M_g}{RT} P_f$ is the gas density, k_f is permeability of fractures and $-Q_{mf}$ is mass the transfer from matrix to fractures.

Similar to the permeability model for the matrix, the permeability of the fracture is also related to the porosity of the fracture (Peng et al., 2016; Harpalani and Schraufnagel, 1990) as

$$\frac{k_f}{k_{f0}} = \left(\frac{\phi_f}{\phi_{f0}} \right)^3 \quad (18)$$

and the porosity of the fracture is related to the effective strain of the fracture as

$$\frac{\phi_f}{\phi_{f0}} = 1 + \frac{\beta}{\phi_{f0}} \Delta \varepsilon_{fe} \quad (19)$$

where ϕ_{f0} is the initial fracture porosity and ϕ_f is the current fracture porosity.

The effective strain of the fracture is also related to the fracture global strain and local force applied by the differential pressure between matrix and fracture. Thus, the effective volumetric strain increment of the fracture is

$$\Delta \varepsilon_{fe} = \Delta \varepsilon_{fv} + \Delta \varepsilon_{fs} - \frac{P_m - P_f}{K_f} - c_{lf} \Delta \varepsilon_{ms} \quad (20)$$

where the first item represents the global strain, which is obtained from the governing equation representing the mechanical deformation of the fracture. The second item represents the sorption-induced strain in the

fracture. The last two items represent the local strains induced by the change of local total stress and local sorption-induced strain of the matrix, respectively. And $c_{lf} = \frac{P_f - P_m}{\Delta P_{max}} \frac{K_m}{K_f}$ is defined as a local strain coefficient.

Substituting Eqs. (19) and (20) into Eq. (18), we now obtain the permeability model of the fracture as

$$\frac{k_f}{k_{f0}} = \left[1 + \frac{\beta}{\phi_{f0}} \left(\Delta \varepsilon_{fv} + \Delta \varepsilon_{fs} - \frac{P_m - P_f}{K_f} - c_{lf} \Delta \varepsilon_{ms} \right) \right]^3 \quad (21)$$

3.4. Determination of fracture system properties

As shown in Eq. (21), a new term, c_{lf} , is defined as a function of the ratio of the matrix bulk modulus, K_m , to the fracture bulk modulus, K_f . Young's modulus (E_m), Poisson ratio (ν_m) and bulk modulus (K_m) of matrix can be obtained through standard mechanical measurements (Wang et al., 2016). Elsworth and Bai (1992) defined a relationship between matrix and fracture properties as:

$$K_f = f(K_m, \alpha_f, \phi_f) = \frac{\phi_f}{\alpha_f - (1 - \phi_f)/K_m} \quad (22)$$

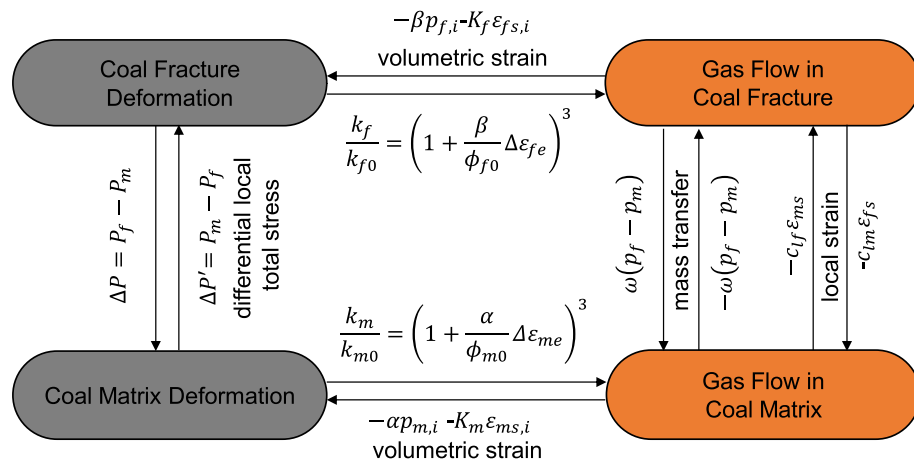
where ϕ_f is the fracture porosity, α_f is fracture-volume compressibility which ranges from $0.000428 \text{ psi}^{-1}$ to 0.00354 psi^{-1} (0.062 MPa^{-1} to 0.51 MPa^{-1}) (Shi and Durucan, 2004; Seidle et al., 1992). Eq. (22) can be used to estimate the bulk modulus for the fracture system. For instance, if $K_m = 10 \text{ GPa}$, $\phi_f = 0.03$ and $\alpha_f = 0.102 \text{ GPa}^{-1}$, then $K_f = 6 \text{ GPa}$.

3.5. Cross-couplings

The mechanisms of gas flow/diffusion in coal and coal deformation are controlled by fully coupled physical fields, as shown in Fig. 3. These continua are connected through a full set of cross-coupling relations, including (a) local force balance between matrix and fractures; (b) local deformation compatibility between the matrix and the fractures; (c) mass exchange between the matrix and the fractures; and (d) sorption-induced strain interactions between fractures and matrixes. And the mechanisms of mass transfer for a dual porosity medium are fluid expansion and viscous displacement. The final form of the transfer function for single-phase flow from matrix to fracture is given as (Ranjbar and Hassanzadeh, 2011)

$$Q = \omega(P_m - P_f) \quad (23)$$

where $\omega = aV\rho_m \frac{k_m}{\mu}$. ρ is the density of the gas, k_m is permeability, μ is viscosity, a is the matrix-fracture transfer shape factor and has dimensions of L^{-2} , P_m is pressure in the matrix, and P_f is pressure in the fracture.



Detailed interactions between different physical fields are summarized as follows:

- (a) The interaction between fracture deformation and gas flow in the fracture is defined by the terms $-\beta P_{f,i}$ and $-K_f \epsilon_{fs,i}$. They represent the change of local effective stress induced by the pressure in the fracture and sorption-induced swelling of the fracture, respectively.
- (b) The interaction between matrix deformation and gas flow in the matrix is defined by the terms $-a P_{m,i}$ and $-K_m \epsilon_{ms,i}$. The first term represents the change of local effective stress induced by pressure in the matrix. The second item represents the change of effective stress induced by swelling of the coal matrix due to gas sorption.
- (c) The interaction between matrix deformation and fracture deformation is defined by the terms $\Delta P_{,i}$ and $\Delta P_{,i}'$. They are equal and opposite. They represent the change in effective stress induced by the change of local total stress applied to matrix and fracture, when the two systems transform from initial equilibrium to the final equilibrium state.
- (d) The interaction between gas flow in the matrix and gas flow in the fracture is defined by the terms $\omega(P_f - P_m)$ and $-\omega(P_f - P_m)$. They represent the gas mass transfer between the two systems.
- (e) The interaction between gas flow in the matrix and gas flow in the fracture is defined by the terms $-c_{lm} \Delta \epsilon_{fs}$ and $-c_{lf} \Delta \epsilon_{ms}$. The first term represents the change in the effective stress of the matrix induced by the local sorption-induced strain of the fracture. Similarly, the second item represents the change in the effective stress of the fracture induced by the local sorption-induced strain of the matrix.

4. Numerical experiments

In order to investigate the performance of the new model under the influence of coupled multiple processes, we apply the model to two common situations: constant confining stress (CCS) and constant volume (CV) conditions. These represent the two endmember conditions. The case of CCS represents free-swelling while the case of CV represents zero-swelling.

4.1. Permeability tests under the condition of CCS

The model geometry of $0.5 \text{ m} \times 1 \text{ m}$ is shown in Fig. 4. For solid deformation, a vertical constraint is applied to the basal boundary while a constant stress of 10 MPa is applied to the other three boundaries. For gas flow, a non-absorbing gas is injected from the upper boundary and flows out from lower boundary. The initial gas pressure in the model and the outlet pressure are both set at atmospheric pressure (101 kPa). Zero flux is specified on the right and left sides of the model. We conduct three experiments with injection pressures of

Fig. 3. Schematic defining cross-couplings among four physical processes: matrix deformation, fracture deformation, gas flow in matrix and gas flow in fracture. The coupling between matrix deformation and fracture deformation is achieved through local force balance. The coupling between matrix deformation and gas flow in the matrix is achieved through volumetric strain (storage change) and permeability evolution. The coupling between gas flow in the matrix and gas flow in fractures is achieved through both gas mass exchange and effective strain compatibility. The coupling between gas flow in the fracture and deformation of the fracture is achieved through volumetric strain (storage change) and permeability evolution.

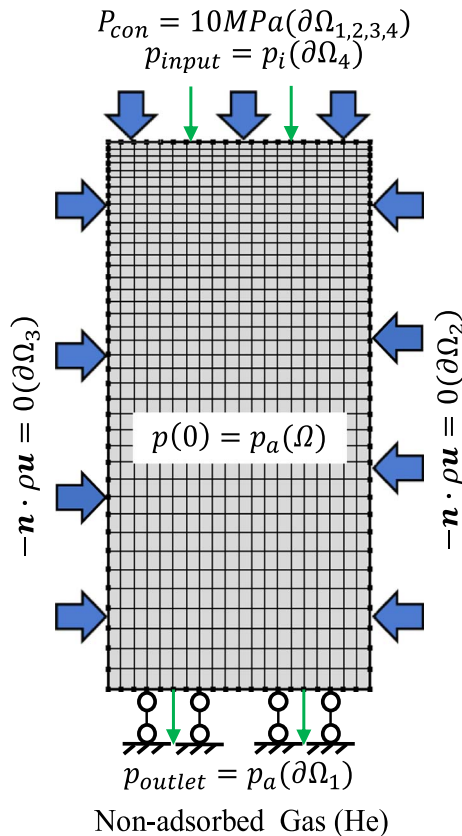
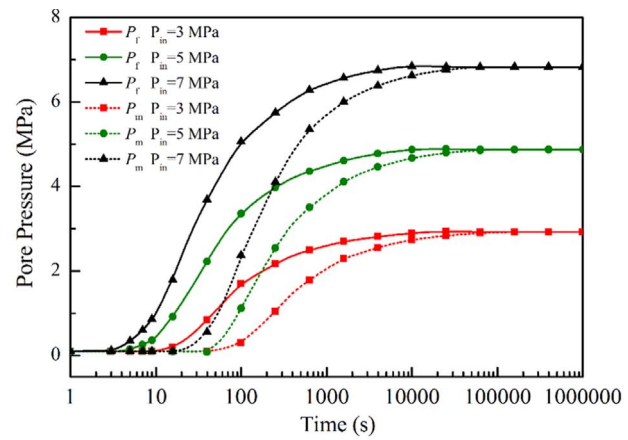


Fig. 4. Simulation model for the case of gas injection under the condition of CCS.

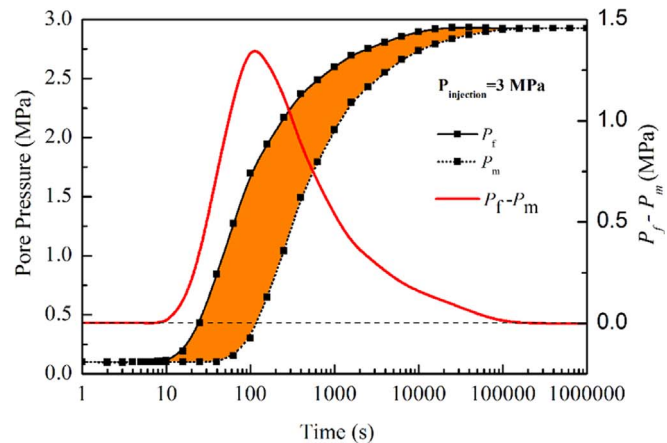
Table 1
Parameters used for the simulation example.

Parameter	Value	Physical meanings	Units
E_m	3	Young's modulus of matrix	GPa
E_f	2	Young's modulus of fracture	GPa
ν_m	0.35	Poisson's ratio of matrix	—
ν_f	0.35	Poisson's ratio of fracture	—
α_m	0.2	Biot coefficient of fracture	—
α_f	0.4	Biot coefficient of matrix	—
μ	1.89×10^{-5}	viscosity	Pas
ϕ_{m0}	0.02	Initial matrix porosity	—
ϕ_{f0}	0.03	Initial fracture porosity	—
k_{m0}	1×10^{-18}	Initial matrix permeability	m^2
k_{f0}	1×10^{-17}	Initial fracture permeability	m^2
P_0	0.1	Initial pressure in the sample	MPa
ρ_m	1500	Matrix medium density	kg/m^3
ρ_f	1290	Fracture medium density	kg/m^3
P_a	0.1	Atmosphere pressure	MPa
ρ_g	0.178	Density of gas at standard conditions	kg/m^3
M	0.004	Molar mass of gas	kg/mol
R	8.314	Gas constant	$\text{J}/(\text{mol}\cdot\text{K})$
T	298.15	Gas temperature	K
P_c	10	Confining pressure	MPa
P_{out}	0.1	Outlet pressure	MPa
a	1	Shape factor	$1/\text{m}^2$
P_{in}	3,5,7	Injection pressure	MPa

3 MPa, 5 MPa and 7 MPa, respectively. The coal properties are as listed in Table 1. For example, the literature values of Poisson's ratio range from 0.2 to 0.5 and the literature values of Young's modulus range from 0.85 GPa to 4.23 GPa (Palmer and Mansoori, 1996; Robertson and Christiansen, 2005; Shi and Durucan, 2005; Wang et al., 2011). For this work, an average value of Poisson's ratio 0.35 was assumed. And we assume the Young's modulus of matrix medium is stronger than fracture's. So, a value of 3 GPa was assumed as coal matrix medium Young's



(a). Evolutions of pressures in matrix and fracture under different injection pressures.



(b) Evolution of the differential pressure with time.

Fig. 5. Evolutions of pressures in matrix and fracture and differential pressure between them during gas injection.

modulus and 2 GPa was assumed as coal fracture medium Young's modulus. Coal densities are selected from the physical properties of sample S3 in Connell et al. (2016). We take solid density as coal matrix medium density while the bulk density as coal fracture medium density.

The evolution of coal permeability and pressure are shown in Fig. 6. For each case, the evolution of pressure and permeability are plotted against time. Modeling results for the case of CCS conditions are shown in Figs. 5–8. In this example, three different injection pressures, from 3 MPa to 7 MPa, were modelled under the same boundary conditions.

The evolution of pressures in matrix and fracture, from the initial equilibrium state to the final equilibrium state, under different injection pressures are shown in Fig. 5(a). For each injection pressure, the fracture pressure increases first and is followed by an increase in the matrix as gas diffuses from fracture to matrix. The evolution of the differential pressure between matrix and fracture is shown in Fig. 5(b). The evolution of the differential pressure, Δp , can be defined as:

$$\Delta p = \begin{cases} 0 & t = t_0^- \\ \Delta p_{max} & t = t_0^+ \\ 0 & t = t_\infty \end{cases} \quad (24)$$

where Δp is the differential pressure between matrix and fracture, and t_0 is the starting time of gas injection. When $t < t_0$ and $t = t_\infty$, there are no differential pressure between the two systems. When $t_0 < t < t_\infty$, the differential pressure acts on the matrix mediums as an external force. However, this force vanishes after the final equilibrium state is reached. When the differential pressure is not equal to

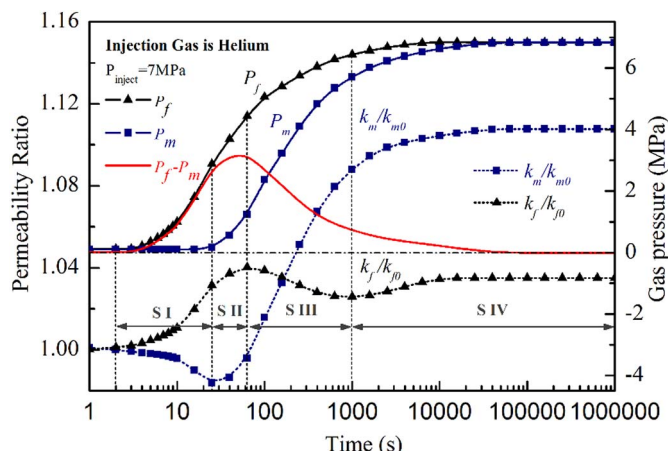


Fig. 6. Evolution of pressures in matrix and fracture, differential pressures between them, and permeability of matrix and fracture during the injection of non-sorbing gas, under conditions of CCS.(For interpretation of the references to color in this figure, the reader is referred to the web version of this article.)

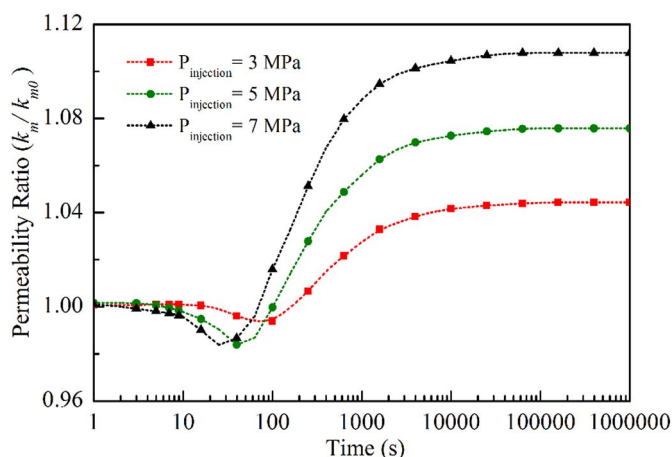


Fig. 7. Evolution of matrix permeability with different injection pressures under the condition of CCS.

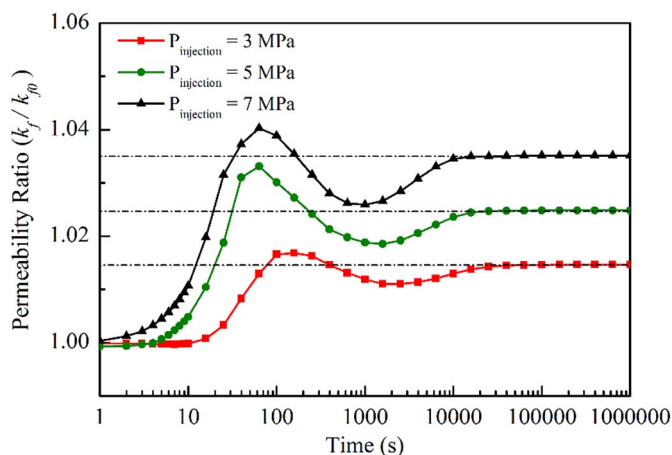


Fig. 8. Evolution of fracture permeability with different injection pressures under the condition of CCS.

zero, it makes the coal matrix deform and affects, in turn, the fracture deformation. We refer to these as “local effects” in this study. These local deformations vanish after the final equilibrium state is reached. These local deformations have significant impacts on the evolution of permeability because permeability is a function of effective strains. In

addition, the differential pressure also controls the gas mass transfer between matrix and fracture systems.

The evolutions of pressures in matrix and fracture, differential pressure and permeabilities of matrix and fracture without the effects of sorption are illustrated in Fig. 6. For the case of gas injection under conditions of constant confining stress, coal permeability normally experiences four stages: In the first stage (S I), the non-adsorbing gas (Helium) flows rapidly into the fracture with little penetration into the matrix medium. The differential pressure increases continuously and reaches a maximum at the end of the second stage. The fracture then swells and permeability of the fracture correspondingly climbs due to the decrease in effective stress induced by the increase in pressure in the fracture. At the same time, the swelling of the fracture applies an extra local force on the matrix medium while the pressure in the matrix changes little. This is why the permeability of the matrix declines slightly at this stage. In this process, the adjustment of the local force balance determines the evolution of both matrix permeability and fracture permeability.

In the second stage (S II), pressure in the matrix increases as gas diffuses from the fracture into the matrix as shown by the blue solid line in Fig. 6. This phenomenon begins locally in the vicinity of the fracture, and gradually expands throughout the entire matrix medium. As a result of this transition, matrix permeability changes from reduction to enhancement. The reason is that the gas-invaded area/volume expands and the increase in pressure in the matrix causes a decrease in the effective stress. Meanwhile, the swelling of the matrix has a negative effect on the evolution of fracture permeability. Subsequently, the fracture permeability decreases when the gas-invaded area is localized in the vicinity of the fractures, and then recovers as the area/volume expands throughout the entire matrix medium. At this stage, local deformations of the coal control the permeability evolution.

In the third stage (S III), pressures in the matrix and fracture are both still increasing but the differential pressure between them switches from an increase to a decline. And the fracture permeability switches from decline to recovery while the matrix permeability increases continuously. These features are caused by the diminishing of local deformation effects. As the gas-invaded area/volume expands, the effective stress in the matrix decreases throughout the entire matrix medium.

When pressures in the matrix equal that in fracture, the system reaches a final equilibrium state and the local effects vanish completely. At this stage (S IV), gas is diffused uniformly within the coal. The fracture permeability stabilizes at a constant magnitude as shown in Fig. 6.

The impacts of injection pressure magnitudes on the evolution of matrix permeability and fracture permeability under the condition of constant confining pressure are shown in Figs. 6 and 7. They all follow the same patterns as described above but the magnitudes of change are different. From the results, we conclude that when the injection pressure is higher, the permeability changes more significantly. This implies that the higher the injection gas pressure is, the greater the influence of local effects.

4.2. Permeability tests under the condition of CV

We generate permeability profiles for another common case under the condition of CV. The model geometry is $0.5 \text{ m} \times 1 \text{ m}$ and the four boundaries of the model are displacement constrained (no deformation), $\mathbf{n} \cdot \mathbf{u}_i = 0$ ($i = 1, 2, 3, 4$) as shown in Fig. 9. The injection gas is non-adsorbing Helium.

Evolution of pressures and permeability are shown in Figs. 10, 11 and 12. Three injection pressures (3, 5, 7 MPa) are used under the same boundary condition. Similar to the case under the condition of CCS, the coal permeability normally experiences three distinct stages. For CCS, the coal permeability experiences four different stages, as shown in Fig. 10: (1) permeability increase due to the sudden increase of fracture

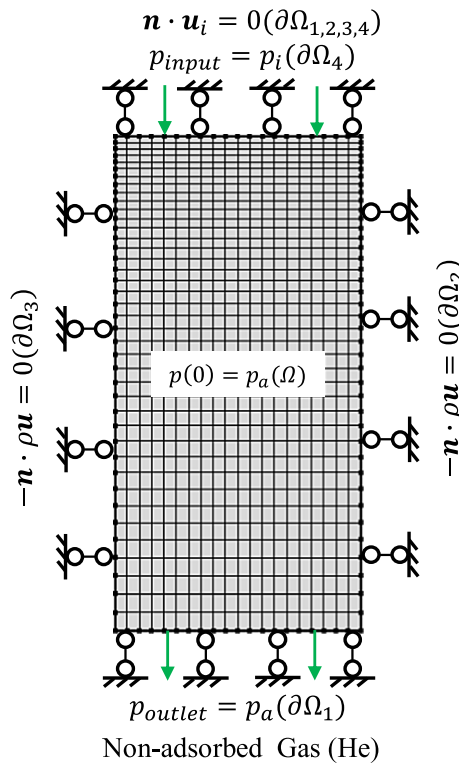


Fig. 9. Model for the case of gas injection under the condition of CV.

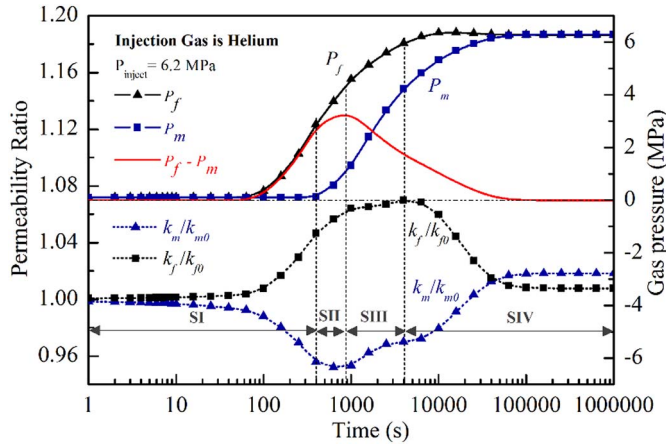


Fig. 10. Evolution of matrix and fracture pressures, differential pressure, matrix permeability ratio, and fracture permeability ratio under the condition of CV.

pressure; (2) permeability decrease as a result of localized matrix deformation; (3) permeability recovery as the matrix deformation expands from local to the entire medium; and (4) permeability stabilization when the pressure in the matrix is equal to that in the fracture. Unlike the case under the conditions of CCS, stage (3) is missing for the case of CV. Under the condition of CV, all matrix swelling is transformed into a reduction in fracture pore space.

4.3. Model verifications against experimental data

We apply the afore-developed permeability models to represent experimental data available from the literature (Robertson and Christiansen, 2005). A series of experiments have been conducted with two different gases, CH_4 and CO_2 , where injection pressure was varied from 100 psia to 800 psia under conditions of constant confining pressure (1000 psia) and temperature (300 K). All permeability

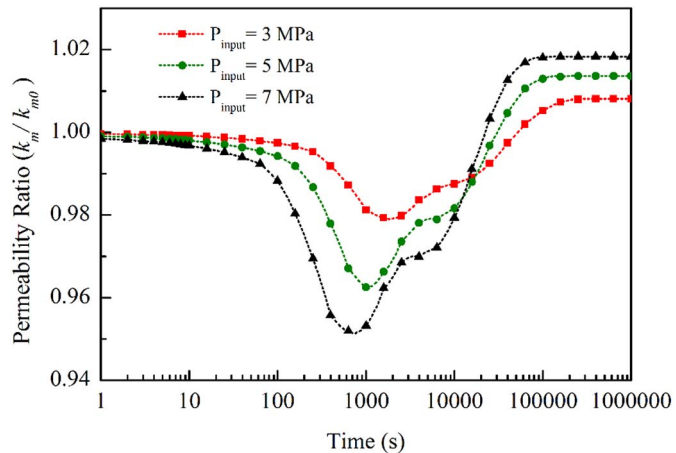


Fig. 11. Evolution of matrix permeability with different injection pressures under the condition of CV.

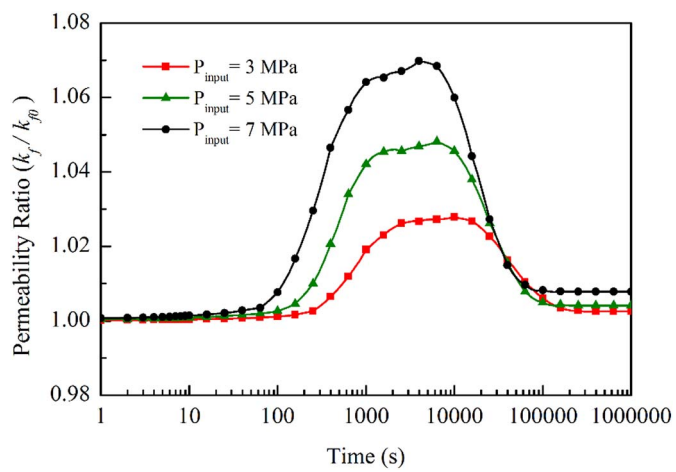


Fig. 12. Evolution of fracture permeability with different injection pressures under the condition of CV.

measurements were conducted at the final equilibrium stages of the experiment. This means that these data points correspond to the magnitudes of permeability data at stage SIV of stabilization in our model as described in Section 4.1. This is an implicit assumption for all current experiments. In this evaluation, we simulated four sets of different experimental data. The modeling steps for all four experimental cases are as follows: (1) we simulate the whole process of each experiment from the initial equilibrium state to the final equilibrium state for each injection pressure; (2) we use a vertical bar to represent the variations of coal permeability at each constant injection pressure; (3) we generate a permeability map for each set of experiments for various injection pressures; (4) we use the permeability map to match the measured permeability curve; and (5) we identify the state of a best-matching point which may not be coincident with the final equilibrium state.

4.3.1. Two experiments on the Anderson coal

For Anderson coal, two experiments were conducted using CH_4 and CO_2 , respectively. We apply the model presented in Section 4.1 to evaluate these two sets of experimental data. All input parameters required for the evaluation are listed in Tables 2 and 3, respectively. In these tables, four parameters for the fractures properties (E_f , ν_f , k_f0 , α_f) are assumed while all others are taken from the literature (Seidle and Huitt, 2018; Connell et al., 2016; Wang et al., 2016).

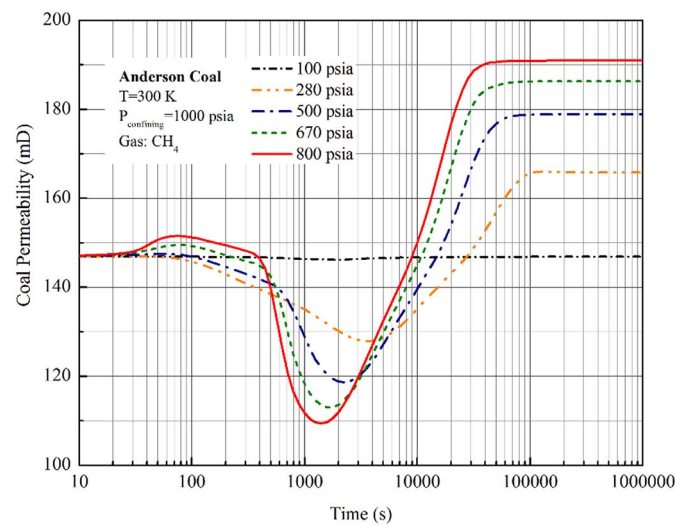
The model results and their comparisons with the experimental data for the case of Anderson coal with CH_4 are shown in Figs. 13 and 14. As shown in Fig. 13, the evolution of permeability during the gas injection

Table 2Parameters used for the case of Anderson coal with CH₄.

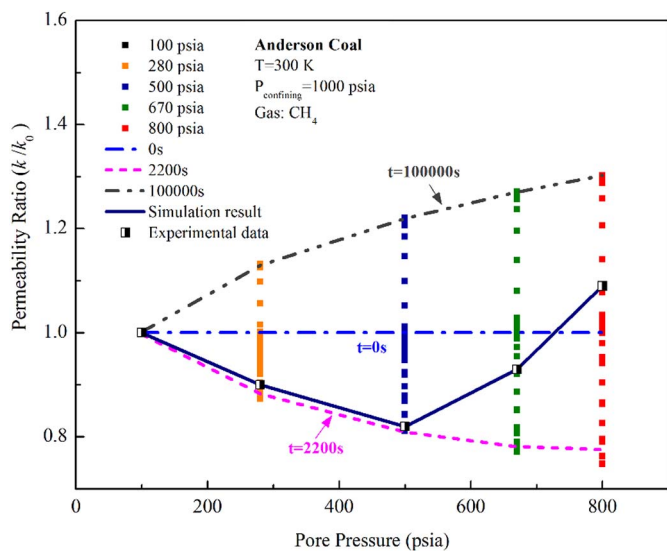
Parameter	Value	Physical meanings	Units
E_m	3.5	Matrix Young's modulus of Anderson coal	GPa
E_f	2.5	Fracture Young's modulus of Anderson coal	GPa
ν_m	0.35	Matrix Poisson's ratio of Anderson coal	–
ν_f	0.4	Fracture Poisson's ratio of Anderson coal	–
α_m	0.6	Biot coefficient of fracture	–
α_f	0.7	Biot coefficient of matrix	–
ρ_g	0.648	Density of CH ₄ at standard condition	kg/m ³
φ_{m0}	0.1	Initial matrix porosity	–
φ_{f0}	0.013	Initial fracture porosity	–
k_{m0}	1.47	Initial matrix permeability	mD
k_{f0}	147	Initial fracture permeability	mD
ρ_m	1250	Matrix medium density	kg/m ³
ρ_f	1000	Fracture medium density	kg/m ³
ε_L	0.0093	Langmuir volumetric strain constant	–
P_L	6.1	Langmuir pressure constant	MPa
μ	11.067	Methane dynamic viscosity	μPa · s

Table 3Input parameters for the case of Anderson coal with CO₂.

Parameter	Value	Physical meanings	Units
E_m	3.5	Matrix Young's modulus of Anderson coal	GPa
E_f	2.5	Fracture Young's modulus of Anderson coal	GPa
ν_m	0.35	Matrix Poisson's ratio of Anderson coal	–
ν_f	0.4	Fracture Poisson's ratio of Anderson coal	–
α_m	0.6	Biot coefficient of fracture	–
α_f	0.7	Biot coefficient of matrix	–
ρ_g	1.784	Density of CH ₄ at standard condition	kg/m ³
φ_{m0}	0.1	Initial matrix porosity	–
φ_{f0}	0.013	Initial fracture porosity	–
k_{m0}	0.86	Initial matrix permeability	mD
k_{f0}	86	Initial fracture permeability	mD
ρ_m	1250	Matrix medium density	kg/m ³
ρ_f	1000	Fracture medium density	kg/m ³
ε_L	0.0353	Langmuir volumetric strain constant	–
P_L	3.82	Langmuir pressure constant	MPa
μ	14.932	Methane dynamic viscosity	μPa · s

Fig. 13. Evolution of permeability with different injection pressures for the case of Anderson coal with CH₄.

process normally experiences four distinct stages: (1) *Stage of Permeability Increase*. Permeability increases in the early stage when the fracture system is filled with the injected gas. This increase in permeability is due to the sudden increase in the injection pressure; (2) *Stage of Permeability Decrease*. Permeability decreases after the pressure in the

Fig. 14. Comparison between experimental data and simulation results for the case of Anderson coal with CH₄.

fracture system reaches the injection pressure. At this stage, gas diffuses from the fracture system into the matrix system. Subsequently, the gas-invaded area/volume in the vicinity of the fracture system swells and this swelling (local deformation) reduces the apertures of fractures. Therefore, the permeability in the fracture system decreases; (3) *Stage of Permeability Recovery*. As the gas-invaded area further expands into the matrix system, the controlling mechanism on the evolution of coal permeability switches from the internal boundary to the external one. Only part of the swelling deformation contributes to the evolution of permeability; and (4) *Stage of Permeability Stabilization*. As the gas-invaded area spreads throughout the matrix system and equilibrium gas pressure between the fracture system and the matrix system is reached, the entire sample swells uniformly. Under this condition, permeability reaches its maximum value. The magnitudes of permeability change are regulated by the injection pressure.

The evolution of coal permeability, as shown in Fig. 13, can be transformed into Fig. 14. We use a vertical bar to represent the variations in permeability with time under a constant injection pressure. The four curves in Fig. 13 becomes four vertical bars in Fig. 14. Unlike previous studies, we present coal permeability as a map not a line. It indicates that the height of the vertical bar is proportional to the magnitude of the injection pressure. For current experiments, only one permeability was measured for a constant injection pressure. This measurement was assumed to represent the permeability at the final equilibrium condition, i.e., the permeability at the fourth stage of stabilization. If this is the case, all measurements should be on the upper limit of the permeability map. If the permeability is not at the upper limit, this suggests that the measurement was taken not at the equilibrium state. Therefore, we can infer the state of an experiment through matching the measured permeability with the modelled one. As shown in Fig. 14, none of the five measured permeability points match with the upper limits on the permeability map. This suggests that all of these measurements were taken under non-equilibrium conditions. This may be due to low matrix permeability.

The model results and their comparisons with the experimental data for the case of Anderson coal with CO₂ are shown in Figs. 15 and 16. The evolution of permeability has a similar trend to the case of Anderson coal with CH₄. They also experience four distinct stages of transformation but the magnitudes are different. Because same parameters were used for the fracture properties, these differences should be caused primarily by the different sorption parameters of the gases.

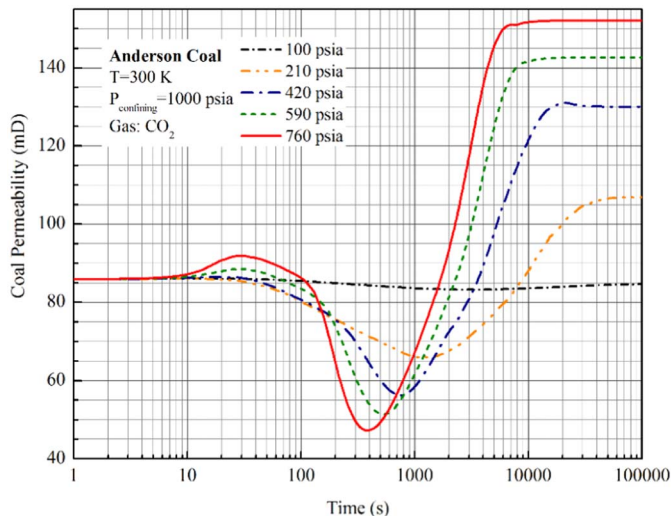


Fig. 15. Evolution of permeability with different injection pressures for the case of Anderson coal with CO_2 .

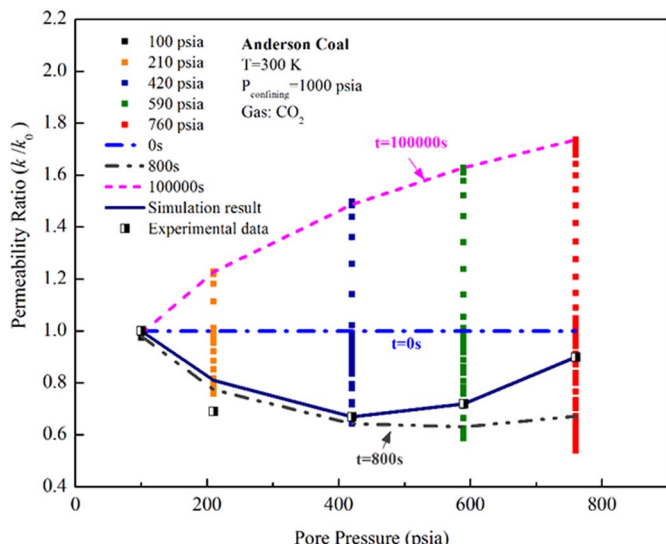


Fig. 16. Comparison of experimental data with simulation results for the case of Anderson coal with CO_2 .

4.3.2. Two experiments on Gilson coal

For Gilson coal, two experiments were conducted, also using CH_4 and CO_2 . We apply the same numerical model, as shown in Fig. 4, to evaluate these two sets of experimental data. All of input parameters required for the evaluation are listed in Tables 4 and 5, respectively. In these tables, four parameters for the fracture properties (E_f , ν_f , k_{f0} , α_f) are assumed while all others are taken from the literature (Seidle and Huitt, 2018; Connell et al., 2016; Wang et al., 2016). The model results and their comparisons with experimental data are shown in Figs. 17–20, respectively. For these simulations, we used the same properties for the fracture system as for the cases of the Anderson coal. The major differences between the Anderson and Gilson coals are defined mainly through three properties, as shown in Table 2. These are the initial matrix permeability, the initial fracture permeability, and the Langmuir strain constants. Through comparison between Figs. 18 and 20, we see that the experimental data are close to the upper boundary of the modelled permeability map for the case of the Gilson coal with CH_4 but are close to the lower boundary for the CO_2 . This is because the Langmuir strain (0.0077) for the former case is much less than (0.0156) for the latter case.

Table 4
Input parameters for the case of the Gilson coal with CH_4 .

Parameter	Value	Physical meanings	Units
E_m	4	Matrix Young's modulus of Gilson coal	GPa
E_f	3	Fracture Young's modulus of Gilson coal	GPa
ν_m	0.35	Matrix Poisson's ratio of Gilson coal	–
ν_f	0.45	Fracture Poisson's ratio of Gilson coal	–
α_m	0.6	Biot coefficient of fracture	–
α_f	0.7	Biot coefficient of matrix	–
ρ_g	0.648	Density of CH_4 at standard condition	kg/m^3
φ_{m0}	0.01	Initial matrix porosity	–
φ_{f0}	0.008	Initial fracture porosity	–
k_{m0}	0.000289	Initial matrix permeability	mD
k_{f0}	0.0289	Initial fracture permeability	mD
ρ_m	1500	Matrix medium density	kg/m^3
ρ_f	1200	Fracture medium density	kg/m^3
ε_L	0.0077	Langmuir volumetric strain constant	–
P_L	6.1	Langmuir pressure constant	MPa
μ	11.067	Methane dynamic viscosity	$\mu\text{Pa}\cdot\text{s}$

Table 5
Input parameters for the case of the Gilson coal with CO_2 .

Parameter	Value	Physical parameter	Units
E_m	4	Matrix Young's modulus of Gilson coal	GPa
E_f	3	Fracture Young's modulus of Gilson coal	GPa
ν_m	0.35	Matrix Poisson's ratio of Gilson coal	–
ν_f	0.45	Fracture Poisson's ratio of Gilson coal	–
α_m	0.6	Biot coefficient of fracture	–
α_f	0.7	Biot coefficient of matrix	–
μ	1.493×10^{-5}	Dynamic viscosity	Pas
ρ_g	1.784	Density of CH_4 at standard condition	kg/m^3
φ_{m0}	0.01	Initial matrix porosity	–
φ_{f0}	0.008	Initial fracture porosity	–
k_{m0}	0.000226	Initial matrix permeability	mD
k_{f0}	0.0226	Initial fracture permeability	mD
ρ_m	1250	Matrix medium density	kg/m^3
ρ_f	1000	Fracture medium density	kg/m^3
ε_L	0.0156	Langmuir volumetric strain constant	–
P_L	3.82	Langmuir pressure constant	MPa
μ	14.932	Methane dynamic viscosity	$\mu\text{Pa}\cdot\text{s}$

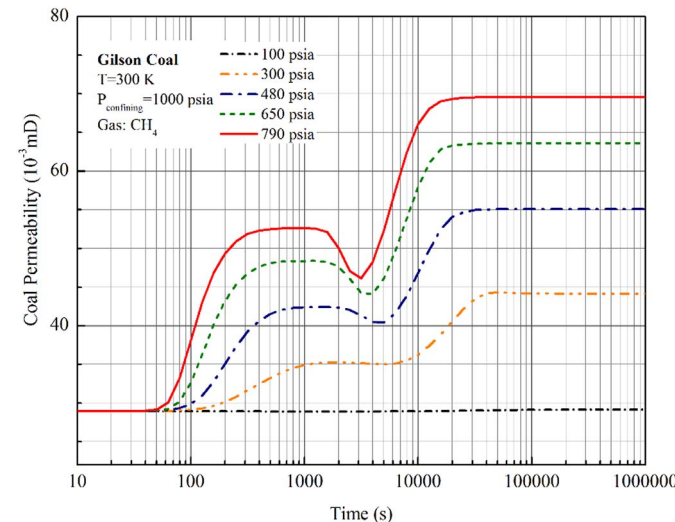


Fig. 17. Evolution of permeability with different injection pressures for the case of Gilson coal with CH_4 .

5. Conclusions

In this study we explore mechanisms of permeability change due to the transition of coal deformation from local (to fracture medium)

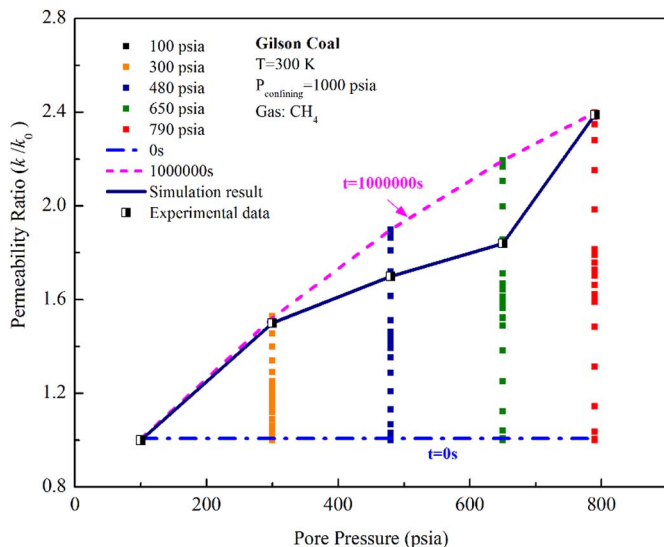


Fig. 18. Comparison between experimental data and simulation results for the case of Gilson coal with CH_4 .

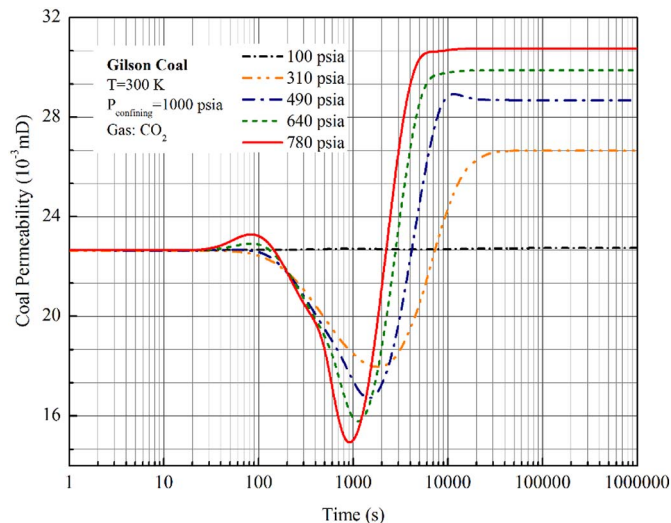


Fig. 19. Evolution of permeability with different injection pressures for the case of Gilson coal with CO_2 .

swelling/shrinking to global (into the matrix medium) swelling/shrinking. This is incorporated into an overlapping continuum approach. Based on the modeling results, the following conclusions are drawn:

- 1) The state of gas pressure equilibrium between matrix and fractures determines whether experimental permeability changes under a constant observed gas pressure or assumed effective stress. If an equilibrium condition is reached, coal permeability is determined by the equilibrium pressure and remains unchanged. If it is not in the state of equilibrium, coal permeability is determined primarily by the dynamics of coal matrix-fracture interactions and evolves with time. This conclusion explains why experimental permeability may change significantly under a constant observed gas pressure or assumed effective stress. For coal seam gas reservoirs, the high contrast between the initial matrix permeability and fracture permeability determines that the evolution processes of both permeability and the associated physical processes from the initial equilibrium state to the final equilibrium state are far more important than these equilibrium states themselves.

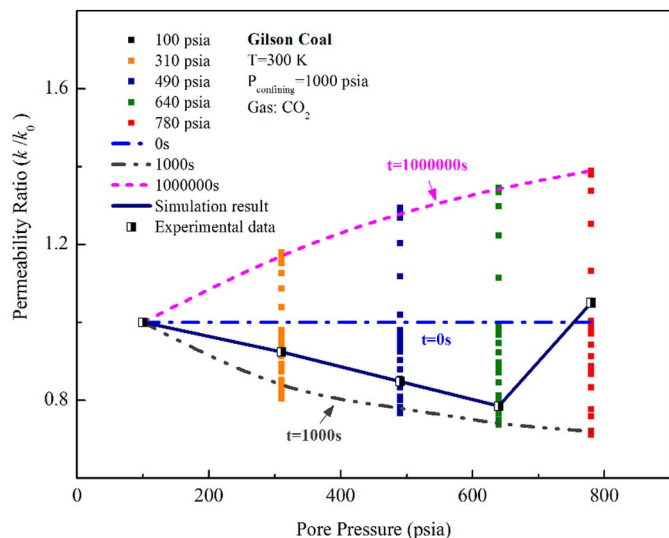


Fig. 20. Comparison between experimental data and simulation results for the case of Gilson coal with CO_2 .

- 2) A typical profile of coal permeability for the case of gas injection experiences four distinctive stages: permeability increase due to the injection pressure, permeability decrease due to local (to fracture) swelling, permeability increase due to the global swelling (into the matrix medium), and permeability stabilization when the final equilibrium is achieved. Depending on the contrast in coal properties, the relative importance of each stage may be different. For example, the stage of permeability decrease due to the local swelling may complete quickly if the matrix permeability is high.
- 3) Coal permeability can be characterized by a map. The upper limit of the permeability is bounded by the solution for free-swelling while the lower limit is set by the solution for the zero swelling (constant volume) case. The variations of permeability between these upper and lower bounds, under a constant gas pressure, are determined by the matrix-fracture interactions, while both the upper and the lower limits are set by the external boundary conditions.

Acknowledgements

This work is a partial result of funding by National Key R&D Program of China (No. 2016YFC0801401) and by the Natural Science Foundation of China (51504235; 51474204) and the 111 Project (B17009). These sources of support are gratefully acknowledged.

References

- Bai, M., Elsworth, D., Roegiers, J.C., 1993. Multiporosity/multipermeability approach to the simulation of naturally fractured reservoirs. *Water Resour. Res.* 29 (6), 1621–1633.
- Chilingar, G.V., 1964. Relationship between porosity, permeability, and grain-size distribution of sands and sandstones. *Dev. Sedimentol.* 1, 71–75.
- Connell, L.D., Mazumder, S., Sander, R., Camilleri, M., Pan, Z., Heryanto, D., 2016. Laboratory characterization of coal matrix shrinkage, cleat compressibility and the geomechanical properties determining reservoir permeability. *Fuel* 165, 499–512.
- Detournay, E., Cheng, A.H.D., 1993. Fundamentals of poroelasticity. In: Fairhurst, C. (Ed.), *Comprehensive Rock Engineering*. Vol. 2. Pergamon, Oxford, pp. 113–171.
- Elsworth, D., Bai, M., 1992. Flow-deformation response of dual-porosity media. *J. Geotech. Eng.* 118 (1), 107–124.
- Gray, R., 1987. Reservoir engineering in coal seams. *SPE Reserv. Eng.* 2 (1), 35–40.
- Guo, P., Cheng, Y., Jin, K., et al., 2014. Impact of effective stress and matrix deformation on the coal fracture permeability. *Transp. Porous Media* 103 (1), 99–115.
- Harpalani, S., Schraufnagel, A., 1990. Measurement of parameters impacting methane recovery from coal seams. *Int. Min. Geol. Eng.* 8, 369–384.
- Liu, H.H., Rutqvist, J., Oldenburg, C.M., 2010a. A new coal-permeability model: internal swelling stress and fracture-matrix interaction. *Transp. Porous Media* 82 (1), 157–171.
- Liu, J., Chen, Z., Elsworth, D., et al., 2011a. Interactions of multiple processes during CBM extraction: a critical review. *Int. J. Coal Geol.* 87 (3), 175–189.

- Liu, J., Wang, J., Chen, Z., et al., 2011b. Impact of transition from local swelling to macro swelling on the evolution of coal permeability. *Int. J. Coal Geol.* 88 (1), 31–40.
- Liu, Q., Cheng, Y., Ren, T., et al., 2016. Experimental observations of matrix swelling area propagation on permeability evolution using natural and reconstituted samples. *J. Nat. Gas Sci. Eng.* 34, 680–688.
- Liu, T., Lin, B., Yang, W., 2017. Impact of matrix–fracture interactions on coal permeability: model development and analysis. *Fuel* 207, 522–532.
- Lu, M., Connell, L.D., 2007. A model for the flow of gas mixtures in adsorption dominated dual porosity reservoirs incorporating multi-component matrix diffusion: part I. Theoretical development. *J. Pet. Sci. Eng.* 59 (1–2), 17–26.
- Lu, M., Connell, L.D., 2010. Swell of coal matrix induced by gas sorption and its partition to pore volume and bulk strains—a critical parameter for coal permeability. In: 44th US Rock Mechanics Symposium and 5th US-Canada Rock Mechanics Symposium. American Rock Mechanics Association.
- Lu, M., Connell, L.D., 2011. A statistical representation of the matrix–fracture transfer function for porous media. *Transp. Porous Media* 86 (3), 777–803.
- Palmer, I., Mansoori, J., 1996. How permeability depends on stress and pore pressure in coalbeds: a new model. *SPE Reserv. Eval. Eng.* 1 (6), 539–544.
- Pan, Z., Connell, L.D., 2007. A theoretical model for gas adsorption-induced coal swelling. *Int. J. Coal Geol.* 69 (4), 243–252.
- Peng, Y., Liu, J., Wei, M., et al., 2014. Why coal permeability changes under free swellings: new insights. *Int. J. Coal Geol.* 133, 35–46.
- Peng, Y., Liu, J., Pan, Z., et al., 2016. Impact of coal matrix strains on the evolution of permeability. *Fuel* 189, 270–283.
- Qu, H., Liu, J., Pan, Z., et al., 2014. Impact of matrix swelling area propagation on the evolution of coal permeability under coupled multiple processes. *J. Nat. Gas Sci. Eng.* 18, 451–466.
- Ramandi, H.L., Mostaghimi, P., Armstrong, R.T., et al., 2016. Porosity and permeability characterization of coal: a micro-computed tomography study. *Int. J. Coal Geol.* 154–155, 57–68.
- Ranjbar, E., Hassanzadeh, H., 2011. Matrix–fracture transfer shape factor for modeling flow of a compressible fluid in dual-porosity media. *Adv. Water Resour.* 34 (5), 627–639.
- Robertson, E.P., Christiansen, R.L., 2005. Modeling permeability in coal using sorption-induced strain data. In: Proceedings of the 2005 SPE annual technical conference and exhibition, Dallas, 9–12 October 2005, paper SPE 97068.
- Seidle, J.P., Huitt, L.G., 2018. Experimental measurement of coal matrix shrinkage due to gas desorption and implications for cleat permeability increases. Paper SPE 30010. In: Proceedings of SPE International Meeting.
- Seidle, J.P., Jeansson, M.W., Erickson, D.J., 1992. Application of matchstick geometry to stress dependent permeability in coals. In: SPE Rocky Mountain Regional Meeting.
- Shi, J.Q., Durucan, S., 2004. Drawdown induced changes in permeability of coalbeds: a new interpretation of the reservoir response to primary recovery. *Transp. Porous Media* 56 (1), 1–16.
- Shi, J.Q., Durucan, S., 2005. A model for changes in coalbed permeability during primary and enhanced methane recovery. *SPE Reserv. Eval. Eng.* 8 (4), 291–299.
- Somerton, W.H., Söylemezoglu, I.M., Dudley, R.C., 1975. Effect of stress on permeability of coal. *Int. J. Rock Mech. Min. Sci. Geomech. Abstr.* 12 (5–6), 129–145.
- Wang, S., Elsworth, D., Liu, J., 2011. Permeability evolution in fractured coal: the roles of fracture geometry and water-content. *Int. J. Coal Geol.* 87 (1), 13–25.
- Wang, J.G., Liu, J., Kabir, A., 2013. Combined effects of directional compaction, non-Darcy flow and anisotropic swelling on coal seam gas extraction. *Int. J. Coal Geol.* 109: 1–14.
- Wang, C., Liu, J., Feng, J., et al., 2016. Effects of gas diffusion from fractures to coal matrix on the evolution of coal strains: experimental observations. *Int. J. Coal Geol.* 162, 74–84.
- Wang, C., Zhai, P., Chen, Z., et al., 2017. Experimental study of coal matrix–cleat interaction under constant volume boundary condition. *Int. J. Coal Geol.* 181, 124–132.
- Wu, Y., Liu, J., Elsworth, D., et al., 2010. Dual poroelastic response of a coal seam to CO₂ injection. *Int. J. Greenhouse Gas Control* 4 (4), 668–678.
- Wu, Y., Liu, J., Chen, Z., et al., 2011. A dual poroelastic model for CO₂-enhanced coalbed methane recovery. *Int. J. Coal Geol.* 86 (2), 177–189.
- Zhang, H., Liu, J., Elsworth, D., 2008. How sorption-induced matrix deformation affects gas flow in coal seams: a new FE model. *Int. J. Rock Mech. Min. Sci.* 45 (8), 1226–1236.